

Supporting information

Promoting effect of Fe modification on the direct synthesis of dimethyl carbonate from CO₂ and methanol over Fe-Ce binary oxide

Lei Dong^{a,b}, Yangyang Yuan^{a,c,*}, Shengjie Zhu^{a,b}, Peidong Li^a, Xiaomin Zhang^a, Yanping Chen^a and Lei Xu^{a,*}

^a National Laboratory for Clean Energy, Dalian Institute of Chemical Physics, Chinese Academy of Sciences, Dalian 116023, PR China.

^b University of Chinese Academy of Sciences, Beijing 100049, PR China.

^c Hangzhou Institute of Advanced Studies, Zhejiang Normal University, Hangzhou 311231, PR China

* Corresponding authors.

Email addresses: yuanyangyang@zjnu.edu.cn, leixu@dicp.ac.cn.

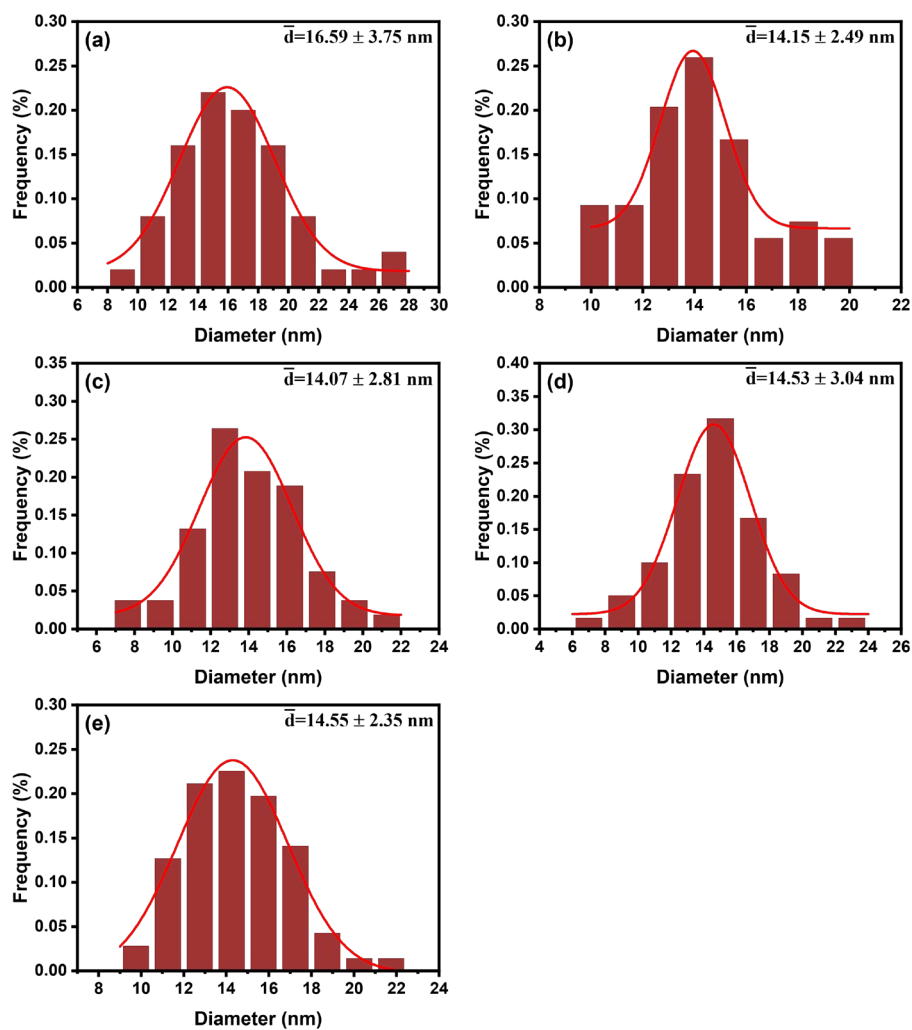


Fig. S1. Particle size distributions of (a) CeO_2 , (b) $\text{Fe}_{0.02}\text{Ce}_{0.98}\text{O}_x$, (c) $\text{Fe}_{0.04}\text{Ce}_{0.96}\text{O}_x$, (d) $\text{Fe}_{0.06}\text{Ce}_{0.94}\text{O}_x$ and (e) $\text{Fe}_{0.08}\text{Ce}_{0.92}\text{O}_x$.

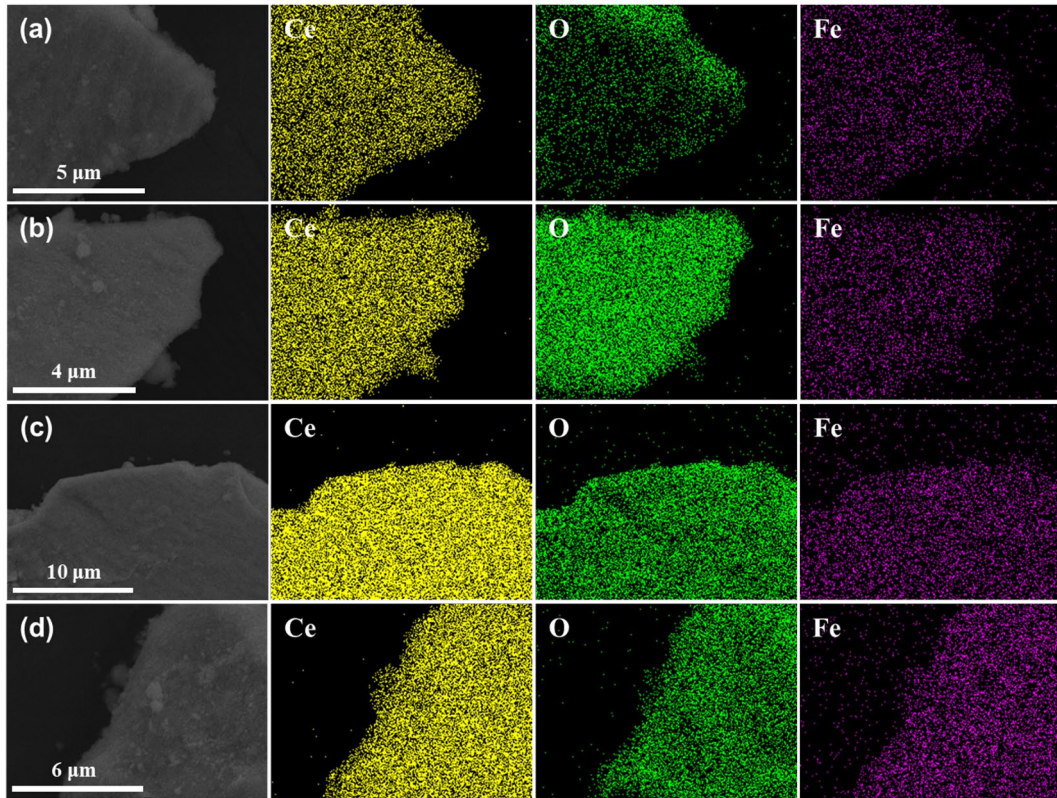


Fig. S2. EDX mapping images of (a) $\text{Fe}_{0.02}\text{Ce}_{0.98}\text{O}_x$, (b) $\text{Fe}_{0.04}\text{Ce}_{0.96}\text{O}_x$, (c) $\text{Fe}_{0.06}\text{Ce}_{0.94}\text{O}_x$ and (d) $\text{Fe}_{0.08}\text{Ce}_{0.92}\text{O}_x$.

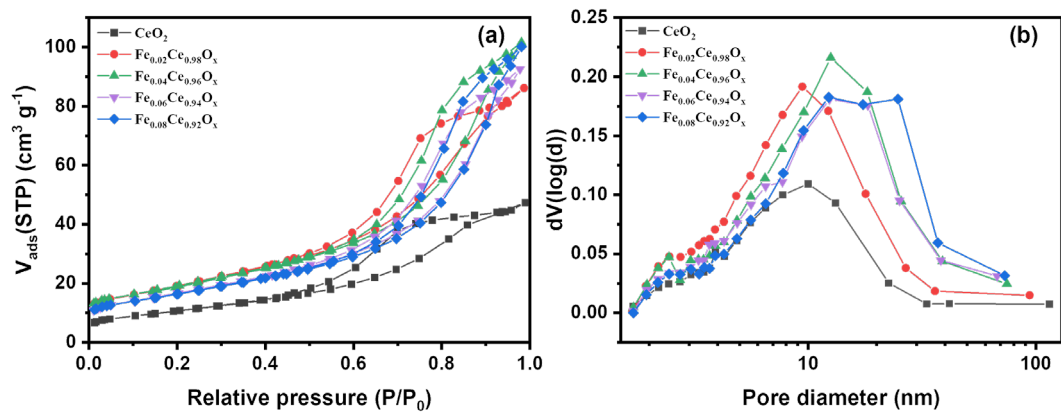


Fig. S3. (a) N_2 adsorption-desorption isotherms and (b) BJH pore size distributions of CeO_2 and $\text{Fe}_\delta\text{Ce}_{1-\delta}\text{O}_x$ catalysts.

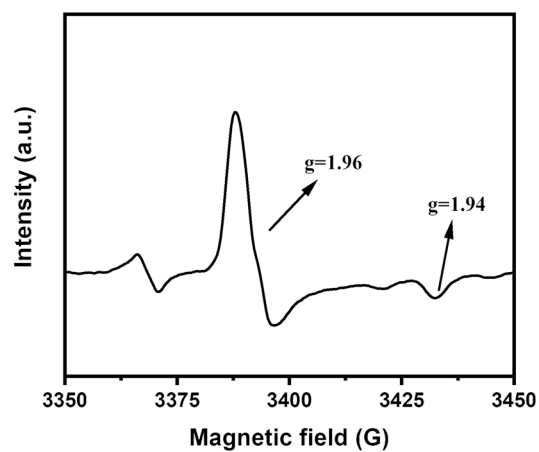


Fig. S4. EPR spectrum of CeO_2 .

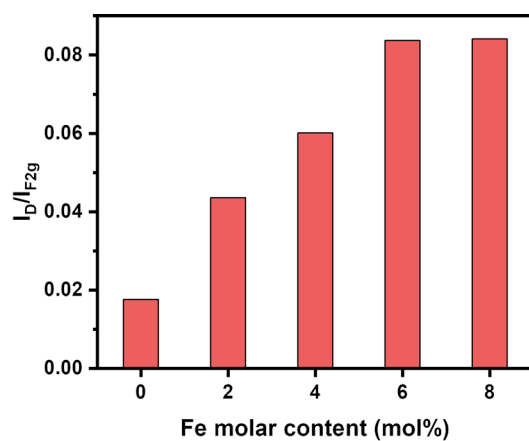


Fig. S5. I_D/I_{F2g} values of CeO_2 and $\text{Fe}_\delta\text{Ce}_{1-\delta}\text{O}_x$ calculated from Raman spectra.

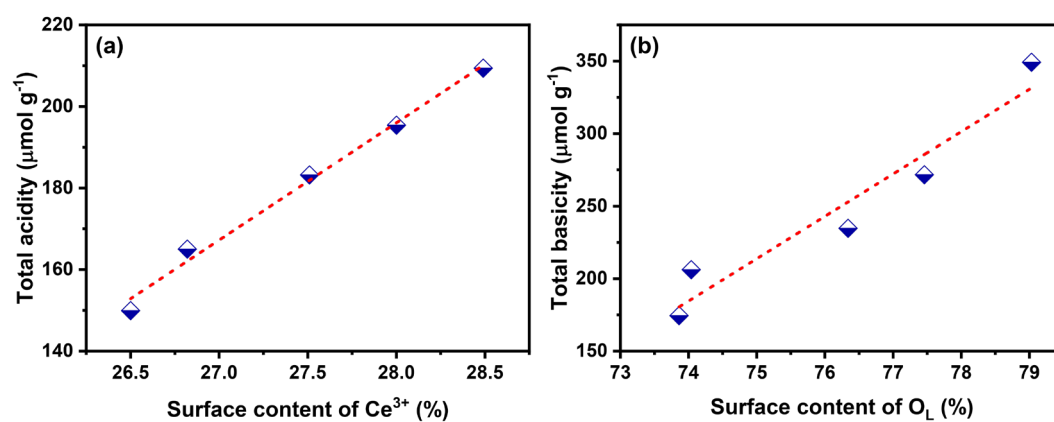


Fig. S6. The relationship between (a) the total acidity and the surface content of Ce^{3+} and (b) the total basicity and the surface content of O_L .

Table S1Catalytic activities of CeO₂ and Fe-modified CeO₂ catalysts for the DMC synthesis.

Entry	Catalyst	2-CP (mmol)	CH ₃ OH conversion (%)	DMC selectivity (%)	STY _{DMC} (mmol g ⁻¹ h ⁻¹)
1	CeO ₂	0	0.27	100.0	2.47
2		50	11.23	99.9	103.93
3	Fe _{0.02} Ce _{0.98} O _x	0	0.37	100.0	3.45
4		50	17.58	99.9	162.71
5	Fe _{0.04} Ce _{0.96} O _x	0	0.41	100.0	3.84
6		50	15.36	99.9	142.73
7	Fe _{0.06} Ce _{0.94} O _x	0	0.36	100.0	3.34
8		50	13.56	99.9	125.88
9	Fe _{0.08} Ce _{0.92} O _x	0	0.34	100.0	3.11
10		50	12.19	99.9	113.11

Reaction conditions: 15 mL of CH₃OH, 0.1 g of catalyst, 3.0 MPa of CO₂ initial pressure, 130 °C, 2 h.**Table S2**Comparison of the catalytic performance of ceria-based catalysts for the direct DMC synthesis from CO₂ and methanol.

Entry	Catalyst	Catalyst amount (g)	Methanol (mL)	CO ₂ initial pressure (MPa)	Temp. (°C)	Time (h)	STY _{DMC} (mmol g ⁻¹ h ⁻¹)	Ref.
1	2%Fe-CeO ₂ (rod)	0.2	30.0	3.0	160	4	0.64	1
2	Ce _{0.9} Fe _{0.1} O ₂ (spindle)	0.3	40.0	4.5	140	3	1.19	2
3	CeO ₂ -Fe ₂ O ₃ (ring)	0.1	15.0	5.0	140	3	1.37	3
4	Fe _{0.7} Zr _{0.3} O _y	1.0	15.0	5.0	110	4	0.11	4
5	Y _{0.5} Fe _{0.5} O _δ -850	1.0	30.0	16.0 (reaction)	240	3	0.51	5
6	SnZr ₄ O _x	0.8	40.0	5.0	140	5	0.14	6
7	Ce _{0.5} Zr _{0.5} O ₂	1.3	25.0	15.0 (reaction)	120	24	0.12	7
8	Ca _{1.5} CeO _x	1.0	35.0	3.0	140	3	0.82	8
9	Ti _{0.04} Ce _{0.96} O ₂	0.2	15.0	5.0	120	5	0.94	9
10	CeO ₂ (nanowire)	0.5	16.0 (g)	5.0	120	5	3.37	10
11	CeO ₂ (quantum dots)	0.01	1.5	5.0	140	2	2.03	11
12	CeO ₂ (Ce-BTC)	0.2	10.0 (g)	5.0	140	4	1.58	12
13	Ce-UiO-66-2	0.1	6.4 (g)	5.5	140	4	0.32	13
14	HPW@MPF-808	0.5	6.4 (g)	12.0 (reaction)	140	4	2.35	14
15	Fe _{0.04} Ce _{0.96} O _x	0.1	15.0	3.0	130	2	3.84	This work

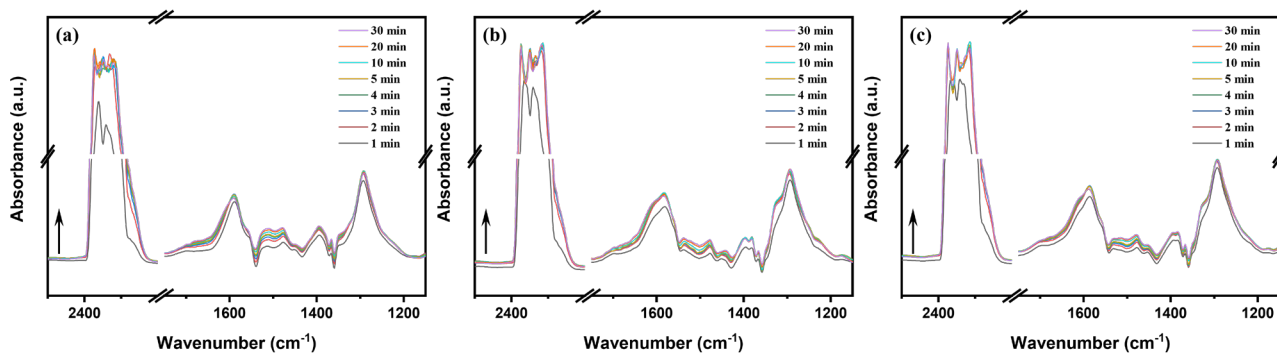


Fig. S7. DRIFTS spectra evolution of CO₂ adsorption on (a) CeO₂, (b) Fe_{0.04}Ce_{0.96}O_x and (c) Fe_{0.06}Ce_{0.94}O_x at 130 °C.

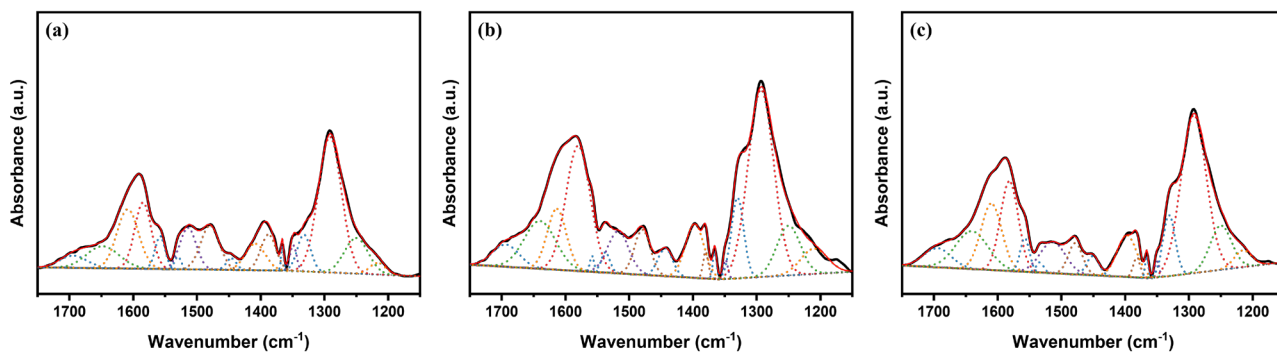


Fig. S8. Resolved IR spectra in the 1750-1150 cm⁻¹ region corresponding to CO₂ adsorption on the surface of (a) CeO₂, (b) Fe_{0.04}Ce_{0.96}O_x and (c) Fe_{0.06}Ce_{0.94}O_x at 130 °C for 30 min.

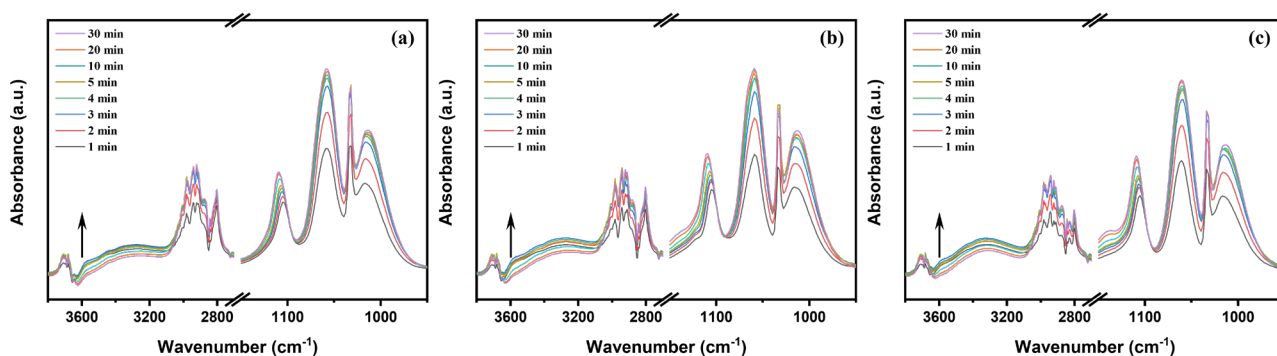


Fig. S9. DRIFTS spectra evolution of methanol adsorption on (a) CeO₂, (b) Fe_{0.04}Ce_{0.96}O_x and (c) Fe_{0.06}Ce_{0.94}O_x at 130 °C.

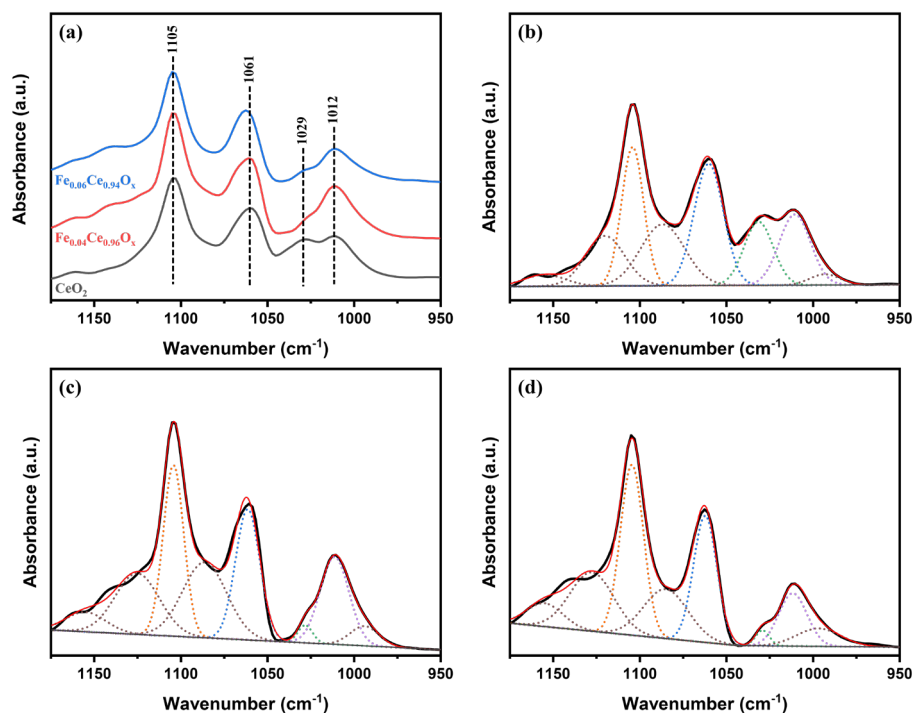


Fig. S10. (a) DRIFTS spectra for CeO_2 and $\text{Fe}_{\delta}\text{Ce}_{1-\delta}\text{O}_x$ after methanol adsorption for 30 min followed by being purged with Ar for 20 min. Resolved IR spectra in the $1175\text{-}950\text{ cm}^{-1}$ region corresponding to the absorption bands of methoxy species on the surface of CeO_2 (b), $\text{Fe}_{0.04}\text{Ce}_{0.96}\text{O}_x$ (c) and $\text{Fe}_{0.06}\text{Ce}_{0.94}\text{O}_x$ (d).

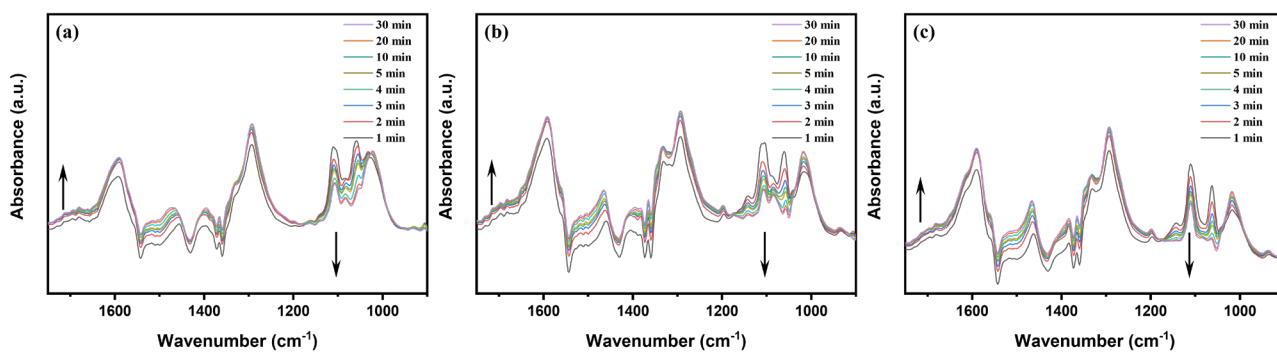


Fig. S11. DRIFTS spectra evolution of CO_2 adsorption on (a) CeO_2 , (b) $\text{Fe}_{0.04}\text{Ce}_{0.96}\text{O}_x$ and (c) $\text{Fe}_{0.06}\text{Ce}_{0.94}\text{O}_x$ pre-adsorbed with methanol at $130\text{ }^\circ\text{C}$.

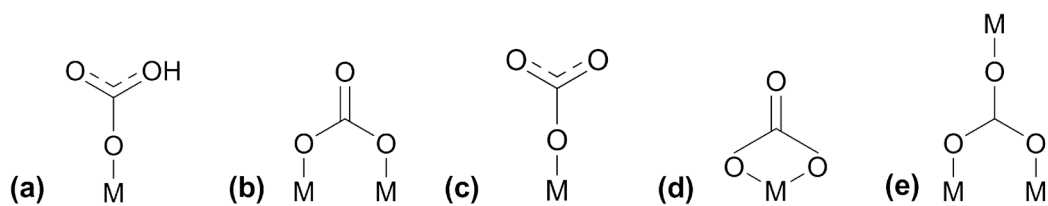


Fig. S12. Schematic illustration of adsorbed carbonate species including (a) bicarbonate, (b) bridged carbonate, (c) monodentate carbonate, (d) bidentate carbonate and (e) polydentate carbonate species.

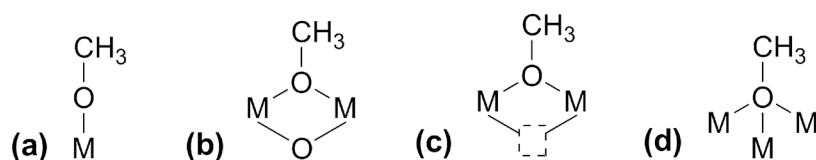


Fig. S13. Schematic illustration of adsorbed methoxy species including (a) terminal methoxy (type I), (b) bridging-I methoxy (type II), (c) bridging-II methoxy (type II') and (d) three-coordinate methoxy (type III) species.

Table S3

Catalytic activities of CeO₂ and Fe-modified CeO₂ catalysts for 2-CP hydration.

Entry	Catalyst	2-CP (mmol)	H ₂ O (mmol)	2-CP conversion (%)	STY _{2-PA+MP} (mmol g ⁻¹ h ⁻¹)	(2-PA+MP) selectivity (%)
1	CeO ₂	50	50	12.47	548.87	100.0
2	Fe _{0.02} Ce _{0.98} O _x	50	50	23.78	1174.16	100.0
3	Fe _{0.04} Ce _{0.96} O _x	50	50	20.44	947.79	100.0
4	Fe _{0.06} Ce _{0.94} O _x	50	50	16.48	806.08	100.0
5	Fe _{0.08} Ce _{0.92} O _x	50	50	14.60	745.40	100.0

Reaction conditions: 15 mL of CH₃OH, 0.01 g of catalyst, 3.0 MPa of CO₂ initial pressure, 130 °C, 1 h.

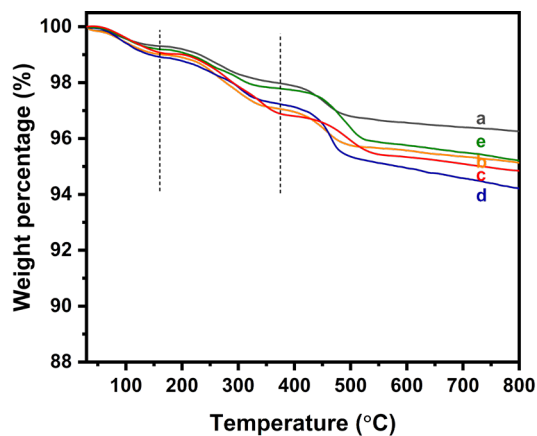


Fig. S14. TG curves of (a) CeO_2 , (b) $\text{Fe}_{0.02}\text{Ce}_{0.98}\text{O}_x$, (c) $\text{Fe}_{0.04}\text{Ce}_{0.96}\text{O}_x$, (d) $\text{Fe}_{0.06}\text{Ce}_{0.94}\text{O}_x$ and (e) $\text{Fe}_{0.08}\text{Ce}_{0.92}\text{O}_x$ pre-treated with the mixture of methanol and 2-CP. The preparation conditions of samples used for the TG test: 0.1 g of catalyst, 50 mmol of 2-CP, 15 mL of CH_3OH , stirring at room temperature, 2 h, methanol washing. Testing conditions: 30 to 800 °C, air, 10 °C min^{-1} .

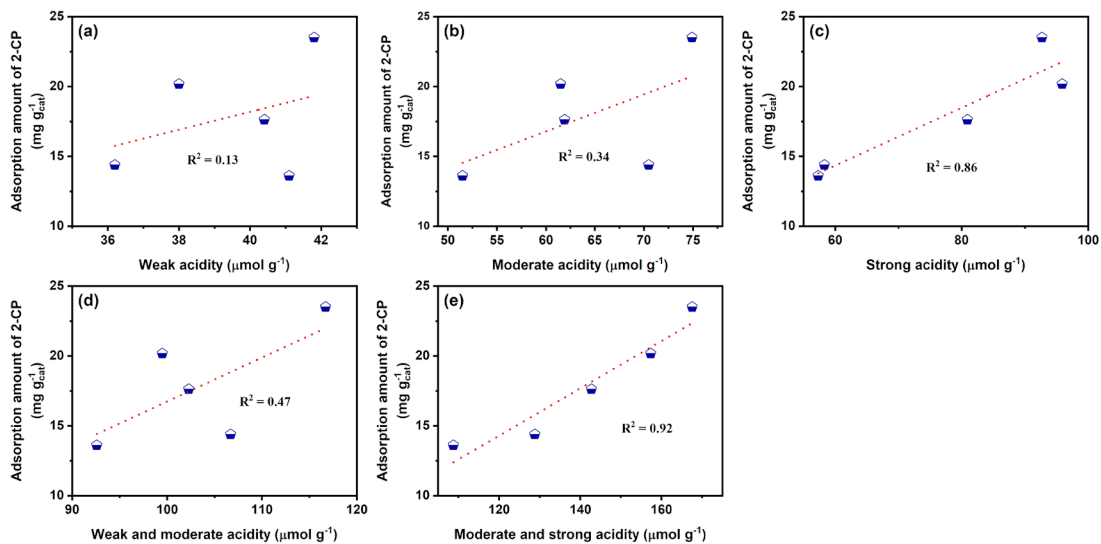


Fig. S15. Correlation between the acidic sites with varying strengths and 2-CP adsorption capacity.

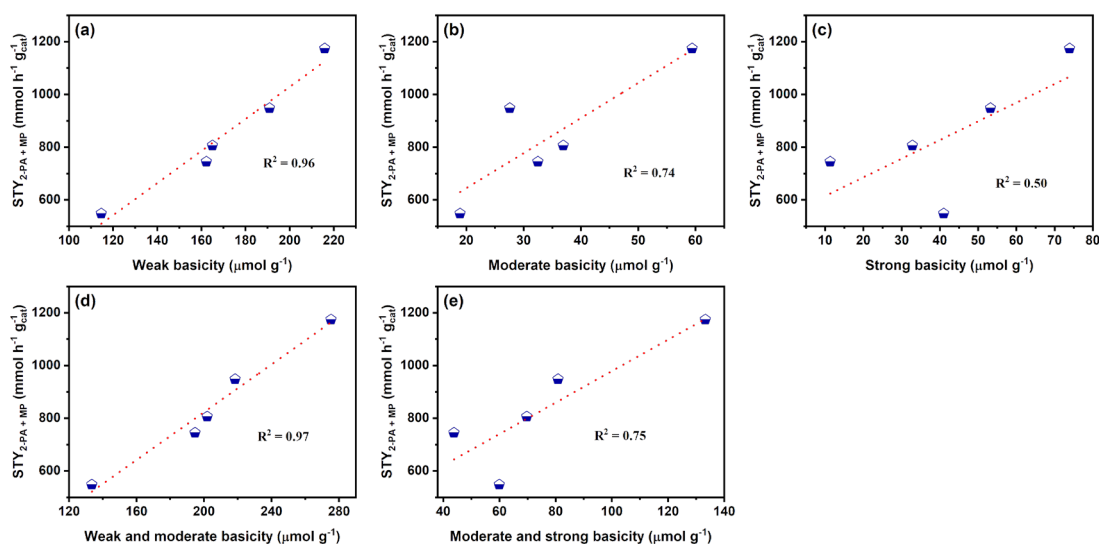


Fig. S16. Correlation between the basic sites with varying strengths and 2-CP hydration activity.

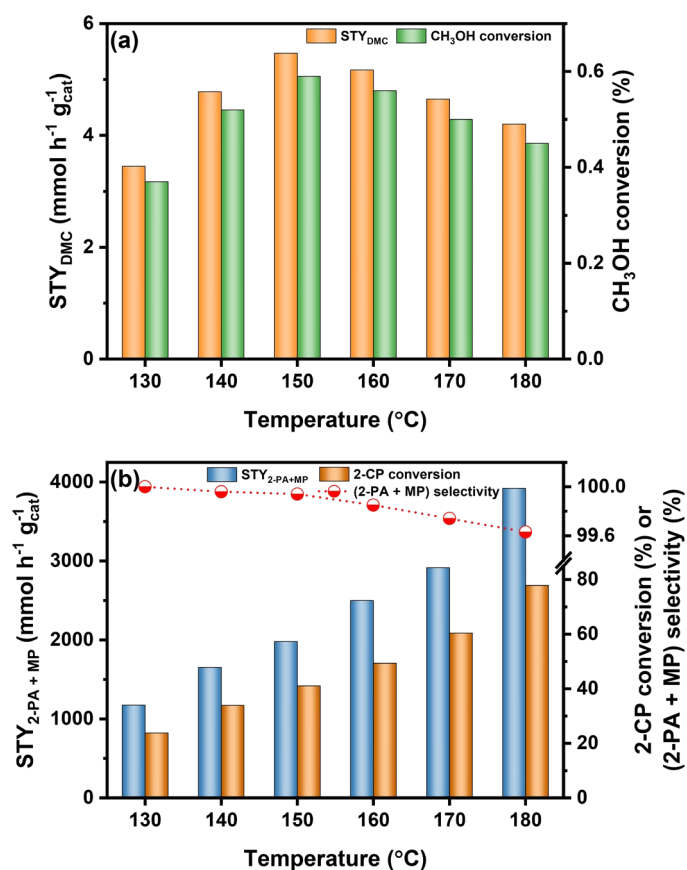


Fig. S17. The effect of reaction temperature on the catalytic performance of Fe_{0.02}Ce_{0.98}O_x for (a) the DMC synthesis from CO₂ and methanol without dehydrating agents and (b) the hydration of 2-CP. Reaction conditions: (a) 15 mL of CH₃OH, 0.1 g of catalyst, 3.0 MPa of pressure, 2 h and (b) 15 mL of CH₃OH, 0.01 g of catalyst, 50mmol of 2-CP, 50 mmol of H₂O, 3.0 MPa of pressure, 1 h.

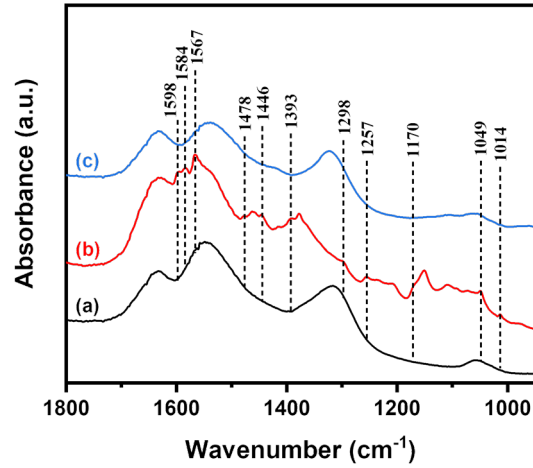


Fig. S18. ATR-IR spectra of (a) the fresh $\text{Fe}_{0.02}\text{Ce}_{0.98}\text{O}_x$, (b) the $\text{Fe}_{0.02}\text{Ce}_{0.98}\text{O}_x$ recycled for four cycles without heat treatment and (c) the $\text{Fe}_{0.02}\text{Ce}_{0.98}\text{O}_x$ regenerated after four cycles by heat treatment.

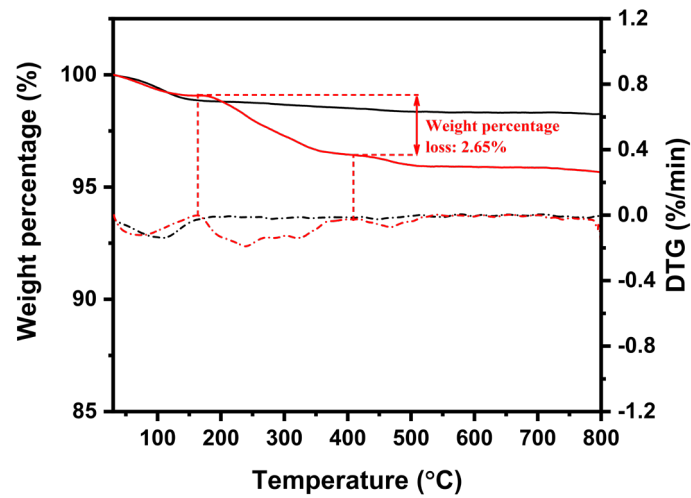


Fig. S19. TG-DTG profiles of the recycled catalysts treated with (black) and without (red) further heat treatment. The solid and dash dot lines represent the TG and DTG curves, respectively.

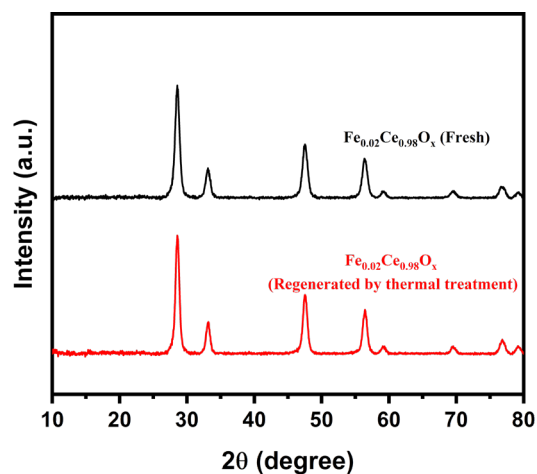


Fig. S20. XRD patterns of the fresh and regenerated $\text{Fe}_{0.02}\text{Ce}_{0.98}\text{O}_x$.

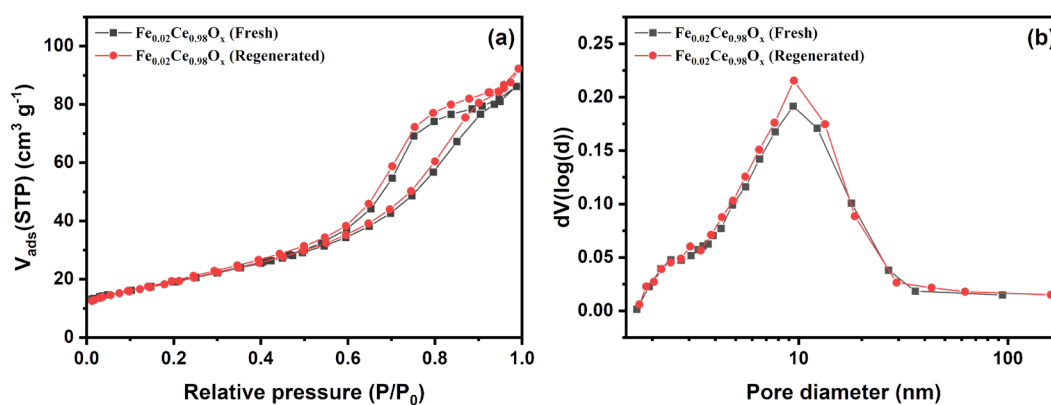


Fig. S21. (a) N_2 adsorption-desorption isotherms and (b) BJH pore size distributions of the fresh and regenerated $\text{Fe}_{0.02}\text{Ce}_{0.98}\text{O}_x$.

Table S4

Textural and compositional properties of the fresh and regenerated $\text{Fe}_{0.02}\text{Ce}_{0.98}\text{O}_x$.

Catalyst	BET surface area ^a ($\text{m}^2 \text{g}^{-1}$)	Pore volume ^b ($\text{cm}^3 \text{g}^{-1}$)	Ce/Fe ratio ^c
Fresh	69	0.13	49.84
Regenerated	70	0.14	49.33

^a Calculated by the Brunauer-Emmett-Teller method.

^b Obtained from the adsorption point at $P/P_0 = 0.99$.

^c Determined by ICP.

References

1. M. Luo, T. Qin, Q. Liu, Z. Yang, F. Wang and H. Li, *ChemCatChem*, 2022, **14**.
2. P. Secharaj, T. Saenman, T. Phiwhom, C. Muangsuwan, S. Srinives and P. Kim-Lohsoontorn, *J. Environ. Chem. Eng.*, 2023, **11**.
3. A. A. Marciniak, E. C. S. Santos, R. J. Caraballo-Vivas, O. C. Alves, M. E. H. Maia da Costa, F. Garcia and C. J. A. Mota, *Energy & Fuels*, 2024, **38**, 628-636.
4. A. Li, Y. Pu, F. Li, J. Luo, N. Zhao and F. Xiao, *J. CO₂ Util.*, 2017, **19**, 33-39.
5. W. Sun, L. Zheng, Y. Q. Wang, W. H. Jia, W. Z. Guo, Z. R. Liu, X. Ding, L. Wu and T. Fang, *J. CO₂ Util.*, 2022, **58**.
6. S. Song, J. Wei, X. He, G. Yan, M. Jiao, W. Zeng, F. Dai and M. Shi, *RSC Adv.*, 2021, **11**, 35361-35374.
7. P. Kumar, P. With, V. C. Srivastava, K. Shukla, R. Gläser and I. M. Mishra, *RSC Adv.*, 2016, **6**, 110235-110246.
8. B. Liu, C. Li, G. Zhang, L. Yan and Z. Li, *New J. Chem.*, 2017, **41**, 12231-12240.
9. Z. Fu, Y. Zhong, Y. Yu, L. Long, M. Xiao, D. Han, S. Wang and Y. Meng, *ACS Omega*, 2018, **3**, 198-207.
10. Z. Fu, Y. Yu, Z. Li, D. Han, S. Wang, M. Xiao and Y. Meng, *Catalysts*, 2018, **8**.
11. Z.-Q. Wang, M.-J. Zhang, X.-B. Hu, V. P. Dravid, Z.-N. Xu and G.-C. Guo, *Chem. Commun.*, 2020, **56**, 403-406.
12. Z. Y. Jiang, S. Y. Zhao, Y. H. Yang, M. H. Tan, G. H. Yang and Y. S. Tan, *Chem. Eng. Sci.*, 2023, **275**.
13. L. Huo, L. Wang, J. Li, Y. Pu, K. Xuan, C. Qiao and H. Yang, *J. CO₂ Util.*, 2023, **68**.
14. K. Xuan, S. Chen, Y. Pu, Y. Guo, Y. Guo, Y. Li, C. Pu, N. Zhao and F. Xiao, *J. CO₂ Util.*, 2022, **59**.